Graphene-gold metasurface architectures for ultrasensitive plasmonic biosensing

Zeng, Shuwen; Sreekanth, Kandammathe Valiyaveedu; Shang, Jingzhi; Yu, Ting; Chen, Chih-Kuang; Yin, Feng; Baillargeat, Dominique; Coquet, Philippe; Ho, Ho-Pui; Kabashin, Andrei V.; Yong, Ken-Tye

2015

Zeng, S., Sreekanth, K. V., Shang, J., Yu, T., Chen, C.-K., Yin, F., et al. (2015). Graphene-gold metasurface architectures for ultrasensitive plasmonic biosensing. Advanced Materials, 27(40), 6163-6169.

https://hdl.handle.net/10356/100121

https://doi.org/10.1002/adma.201501754

ADVANCED MATERIALS WILEY-VCH

DOI: 10.1002/adma.201501754
Article type: Communication

Graphene-gold Metasurface Architectures for Ultrasensitive Plasmonic Biosensing

*Shuwen Zeng, Kandammathe Valiyaveedu Sreekanth, Jingzhi Shang, Ting Yu, Chih-Kuang Chen, Feng Yin, Dominique Baillargeat, Philippe Coquet, Ho-Pui Ho, Andrei V. Kabashin and Ken-Tye Yong**

[*] Prof. K.-T. Yong, Corresponding-Author, Dr. S. Zeng, Prof. D. Baillargeat, Prof. P. Coquet
CINTRA CNRS/NTU/THALES, UMI 3288, Research Techno Plaza, 50 Nanyang Drive, Border X Block, Singapore, 637553
Email: ktyong@ntu.edu.sg
Dr. S. Zeng, Dr. F. Yin, Prof. K.-T. Yong
School of Electrical and Electronic Engineering, Nanyang Technological University, Singapore, 639798
Dr. K.V. Sreekanth, Dr. J. Shang, Prof. T. Yu
Division of Physics and Applied Physics, School of Physical and Mathematical Sciences, Nanyang Technological University, 21 Nanyang Link, Singapore, 637371
Prof. A.V. Kabashin
Aix Marseille University, CNRS, LP3 UMR 7341, Campus de Luminy, 163 Avenue de Luminy, Case 917, 13288, Marseille cedex 9, France
Dr. C.-K. Chen
The Polymeric Biomaterials Lab, Feng Chia University, Taichung, Taiwan 40724
Prof. H.-P. Ho
Department of Electronic Engineering, The Chinese University of Hong Kong, Hong Kong
Prof. P. Coquet
Institut d'Electronique, de Microélectronique et de Nanotechnologie (IEMN), CNRS UMR 8520 – Université de Lille 1, 59650 Villeneuve d'Ascq, France
Prof. D. Baillargeat
XLIM UMR CNRS 7252, Université de Limoges/CNRS, Limoges 87060, France

Keywords: surface plasmon polaritons, metasurfaces, plasmonic sensing

With spectacular progress of surface plasmon resonance and localized plasmon resonance-based sensing modalities for last years, plasmonic biosensing has become the core label-free technology for studies of biomolecular interactions.[1,2] Despite a series of advantages offered by direct, label-free detection, plasmonic technology still needs a drastic improvement of sensitivity to match requirements of many critical areas of biomedical research, including early disease diagnostics and pharmacology.[3-5] Here, we describe novel hybrid graphene/gold metasurface architectures for plasmon excitation, which can provide a

significant gain in sensitivity and give access to the detection of trace amounts of target analytes. Benefiting from extreme singularities in phase of reflected light as a result of plasmon field enhancement on the graphene sheet and a strong plasmon-mediated energy confinement, the metasurface demonstrates much improved sensitivity to refractive index variations nearby and to the attachment of signal-enhancing Au nanoparticle tags. Running a protocol of single-stranded DNA (ssDNA) on graphene/gold metasurface, we report the sensitivity of 1 aM (10^{-18} M), which is 3 orders of magnitude higher than any state-of-the-art plasmonic sensors. Combined with the ability of graphene-based substrate to selectively absorb some molecules through pi stacking forces, the proposed metasurface architecture provides a unique platform to selectively detect aromatic rings structure biomolecules (e.g. DNA, RNA, peptides and cytokines). Our proof-of-concept results offer a pathway toward simple and scalable technology for the detection of trace amounts of analytes.

Surface Plasmons are oscillations of free electrons in metals, which exist at the metal/dielectric interface and can be optically excited over thin metal films and nanostructures.[1-3] Electric field associated with these oscillations decays exponentially into the dielectric medium making plasmons extremely sensitive to refractive index of this medium. This remarkable property has been employed in Surface Plasmon Resonance (SPR) biosensors,[4-6] which rely on the control of biological binding/recognition events on a thin gold film via refractive index monitoring. The attachment of the target analyte to a gold-supported receptor causes a perturbation of plasmon electric field, which is normally monitored by following angular or spectral position of the plasmon-related feature in reflected light. Similar effect can be obtained with localized plasmons over metal nanostructures in conditions of Localized Plasmon Resonance (LPR).[3, 7] It is important that both modalities can avoid expensive, time-consuming and precision-interfering labeling steps to mark analytes, while their high sensitivity is due to strong plasmon-related probing field and a resonant nature of its response. Despite significant progress for last couple of decades, both modalities of plasmonic sensors still need a drastic

improvement of sensitivity to compete with classical labeling approaches. The detection limit of SPR biosensors in terms of the amount of a biomaterial accumulated on the surface is of the order of 1 pg/mm^2 (for LPR biosensors the relevant value is about 1000 pg/mm^2) that is inferior by 2 orders of magnitude to labeling methods.[6, 8] As an example, current SPR setups are not able to detect low molecular weight molecules such as DNA, cytokine and hormones especially at concentration below 1fM, which is 1-2 orders of magnitude higher than required in many tasks of early-stage disease diagnostics.[8, 9]

Such a lack in the detection limit compared to classical labeling methods can be gained up by passing from amplitude to phase characteristics of light.[10-12] As phase is not determined in the point where reflected intensity is equal to zero (point of darkness),[13] it can experience a sharp jump under SPR and this jump can be employed as a sensing parameter. Here, a much superior phase sensitivity compared to the amplitude one is largely due to field intensity factor: the phase jump takes place in the very minimum of the SPR curve where probing electric field is maximal while relevant change of amplitude characteristics occurs in its slopes where probing field is much weaker.[13] In this case, lower in the intensity of light at the point of resonance (darker is the structure), stronger is the probing field and sharper is the phase jump. Although Fresnel's formulae predict infinite Heaviside-like phase behavior under a proper selection of gold film thickness under SPR,[13] this singularity never happens in practice due to non-zero film roughness and the reflected intensity inside the dip is normally not lower than 3-5%. One of solutions of this problem of conventional materials consists in involving metamaterials, or artificial materials composed of properly arranged metal nanodots (metaatoms) with nanoscale distance between them, which can provide controlled photonic response or new sensing functionalities.[2, 14] It has been recently shown that a proper design of metamaterial supporting diffraction-coupled plasmons can lead to complete darkness, yielding to extreme phase singularities.[7] The employment of such phase singularities opens up access to single molecular label-free detection with spectacular opportunities for the improvement of current state-of-the-art biosensing technology.[7]

In this communication, we explore other routes to implement improved phase sensitivity and focus our attention to graphene plasmonics.[15-19] It has been recently shown that the presence of graphene layers on gold can result in an improved sensing response in conventional SPR and opens access to new functionalization strategies through pi stacking interactions.[20-22] We show that graphene plasmonics structures can provide extreme phase features as a result of electric field enhancement, offering much improved phase sensitivity. We additionally consider graphene plasmonics architecture with gold nanoparticle-based enhancement to further improve the sensing response.[23] The recorded sensitivity of 1 aM (10^{-18} M) for detecting single-stranded DNA (ssDNA) appears to be far beyond relevant values for any state-of-the-art plasmonic sensors available in the markets and bench side prototypes.[5, 6, 24] Presenting an Au-perturbed single layer honeycomb lattice of C atoms, the graphene/gold interface fits the definition of "metasurfaces" to provide a drastic concentration of plasmon electric field in 2D plane as a novel functionality.[25, 26]

In the basic geometry, the proposed metasurface architecture consists of a gold film coated by a single (or multi) sheets of Graphene, as shown in **Figure 1**a. The layer/layers of graphene is/are deposited in such a way that graphene and gold are in full electric contact. In another gold nanoparticle-enhanced geometry, spherical Au nanoparticles are additionally employed as amplification tags to enhanced SPR sensing response, as shown in Figure 1b. Both cases imply the excitation of Surface Plasmon Polaritons over the Graphene/Gold Interface that can be done e.g. with a prism coupling scheme using the Kretschmann-Raether arrangement (Figure 1a,b). Under the production of Surface Plasmon Resonance, the distribution of electric field is characterized by an exponential decay toward both gold film and adjacent dielectric medium, respectively. In this case, the presence of Graphene sheets leads to a strong localization of the field at the graphene-gold interface, as shown in Figure 1c, and a drastic field enhancement. Figure 1e illustrates the field enhancement effect under the deposition of different numbers of graphene layers on the gold surface. It is visible that more

than 4-fold enhancement of electric field takes place under the deposition of a single graphene layer on gold, while a further deposition of layers (2 ones and more) does not provide the field enhancement effect. **Figure 2**a illustrates the behavior of amplitude and phase parameters of light reflected under SPR. One can see that phase experiences a sharp "Heaviside-like" singularity in the very minimum of the SPR curve (point of light "darkness"),[7] where the probing electric field is maximum. It is worth noting that the conventional SPR detection method based on the angular measurement is strongly dependent on the plasmon damping of the graphene layers due to their absorbing dielectric property. In this case, the signal change (i.e., the resonance angle change) to the surrounding environment increases with the number of graphene layers.[20] However, more graphene layers would result in electron energy loss of the excited SPR electric field. This will increase the full width at half maximum (FWHM) of the SPR curves and thus significantly reduce the SPR detection resolution.[20, 27] For the phase detection approach, the signal change (i.e., the phase jump at the resonance angle) is only dependent on the minimum reflectivity of the SPR curves. Thus, when the value of the minimum reflectivity is lowered, the change of the phase signal becomes larger. When the reflectivity has the lowest value, the intensity of the excited electric field will reach a maximum value which means that almost all the incident light energy (~100%) has been successfully transferred to the resonance energy of the SPR waves. As shown in Figure 2b, the response of phase to variations of refractive index of the adjacent dielectric medium appears to be directly proportional to the intensity of the probing field at the graphene-gold interface: it is more than 4-fold enhanced when single layer of Graphene is deposited on the gold surface, while the deposition of 2 and more graphene layers does not improve the resulting sensitivity. An additional employment of Au tags (Figure 1b) leads to a further local enhancement of probing electric at the point of their attachment of the metasurface and this event leads to a local redistribution of electric field pattern (Figure 1d). In our analysis, we also examined local electric field enhancement due to the attachment of gold nanoparticles of different sizes. We found that the best 40-fold enhancement takes place when 30-nm nanoparticles are used (Supporting Information

Figure S3, S4): this effect is attributed to the highest absorption efficiency and lowest scattering efficiency of the 30 nm Au nanoparticle when they are coupled to the graphene coated-Au thin film.[28] Giovannetti et al. reported that electrons would transfer from graphene to the surface of Au thin film in order to maintain the continuity of the Fermi levels when they contact with each other, as the work function of Au (5.54 eV) is larger than that of graphene (4.5 eV).[29] Therefore, the charge transfer is one of the main reasons for the SPR field enhancement which is induced by the graphene layers. Moreover, the excited plasmons at the graphene surface have a sensitive response towards the effective dielectric constant change of the surrounding environment. And all these factors contributed to the strong enhancement in the detection sensitivity of our proposed sensing system. Single graphene layer is also known to absorb 2.3% of transmitted light and lead to a certain loss of light intensity,[30, 31] which could explain the decrease of SPR sensitivity and field intensity when the number of graphene layers coated on the Au sensing film is larger than 2.

To confirm the consistency of the proposed concept and the validity of our calculations, we fabricated a monolayer graphene-coated Au sensing film and compared its sensing performance with that of the bare Au thin film by using a home-built differential phase-sensitive SPR sensor (see details in the Supporting Information Section 2.3). The large area monolayer graphene (~ 1.5cm × 1.5cm) was grown on a high-purity copper foil by using a low-pressure chemical vapor deposition method and it was transferred from the copper substrate to a 50-nm Au thin film. A 2.5 nm layer of Ti was placed between the Au film and the glass substrate in order to improve the adhesion of gold. Aqueous solutions of glycerin with different weight ratios were pumped into the SPR flow cell and interacted with the monolayer graphene-coated Au thin film and bare Au thin film, respectively. Figure 2c shows the responses of phase to a gradual increase of concentration of glycerine: 0.25%, 0.5%, 1%. It is visible that in this range of chosen concentrations phase response is directly proportional to the concentration, while a relatively low level of experimental noises illustrates the potential of the chosen phase-sensitive instrumental scheme for achieving relatively low detection limit values. Figure 2d

compares phase responses of graphene-coated and pure Au film to refractive index variations, as calculated from the glycerin calibration measurements. One can see that both geometries evidence a gradual linear change of phase under the increase of refractive index. Such signal changes become saturated when the shift of refractive-index is larger than 10^{-3} RIU. However, the phase response of graphene-gold metasurface geometry appears to be about 4-times stronger compared to the pure gold film case, which is in excellent agreement with our theoretical estimations of sensitivity and field enhancement gains, as shown in Figure 2b and Figure 1e, respectively. As it has been experimentally shown,[10, 12, 13] the employment of phase as a sensitive parameter can lead to the detection limit as low as 10^{-8} Refractive Index Units (RIU) that is more than 1 order of magnitude better compared to conventional SPR employing amplitude parameters (resonant angle of incidence or wavelength). Therefore, the reported 4-times increase of sensitivity through the employment of graphene-gold architecture opens up the possibility for lowering of the detection limit of phase-sensitive SPR down to 10^{-9} RIU, which promises the detection of trace amounts of biomolecules down to single molecular level.[7] It should be noted that due to the employment of phase as a sensing parameter our sensitivity is far beyond all values reported with graphene-enhanced SPR sensing schemes.[16, 18, 20, 32] In general, the proposed graphene-gold metasurface architecture offers a very efficient approach for the implementation of extreme phase singularities. Similar effect was recently recorded using gold nanodot array-based metamaterials based on diffraction coupling of localized plasmons.[7] Both approaches reveal a drastic sharpening of phase features due to the enhancement of electric field intensity in the sensing interface. As it was shown in Ref. 7, this phenomenon is accompanied by near-zero intensity reflection (light darkness).

It is important that the proposed graphene-gold metasurface-based biosensing approach offers novel surface chemistry functionalization strategies, which can provide decisive advantages over conventional SPR for many biosensing tasks. In particular, aromatic ring structure biomolecules such as helical peptides or proteins can selectively bind to the surface of graphene due to pi-stacking

interactions,[21, 22] as illustrated in **Figure 3**a, whereas conventional SPR sensors that use bare Au sensing film requires tedious surface functionalization steps to accomplish the same task. To assess the efficiency of such functionalization strategy, we tested the proposed metasurface architecture in a model of single-stranded DNA, which can adsorb on graphene through the pi-stacking interactions: this mechanism renders possible a much more efficient binding of ssDNA to graphene compared to double-stranded DNA.[22] In our tests, we pumped 7.3kDa 24-mer ssDNA solutions of different concentrations ranging from 100 aM to 100 nM into a flow cell contacting with the graphene-gold metasurface (Supporting Information Section 2.3.3). The size of our flow chamber is 1.5 cm × 1.5 cm × 0.5 cm and the diameter of 785 nm laser spot is 1 mm. The solutions containing ssDNA molecules were injected into the chamber from the bottom and once the chamber was filled up, the injection was stopped to allow a complete interaction to take place between the ssDNA molecules and the graphene-coated sensing film. The laser spot was focused at the center of the interaction area. Each time before injection, a calibration process as shown in Figure 2c was carried out to check and confirm the quality of the monolayer graphene-coated sensing substrate. As shown in Figure 3b, Supporting Information Figure S8 and S9, we could observe phase signal changes upon introducing the ssDNA solutions onto the sensor head, which corresponded to the binding of ssDNA on the monolayer graphene-coated sensing substrates. After 8 min reaction time, DI water was injected into the system to remove any unbound and weakly attached ssDNA and this step resulted in a slight decrease and stabilization of the signal. Longer immersion time did not affect the signal change. To further improve the SPR sensitivity, we used an additional step, which implies the employment of Au nanoparticles to enhance the resulting signal (Figure 1b). Solutions containing positive-charged 30-nm Au NPs of identical optical density were supplied onto the ssDNA-modified sensing substrate. Since zeta potential of desalted ssDNA solution was measured to be negative, strong electrostatic bindings occurred when they interacted with the positively-charged Au NPs. After a few minutes of reaction time, DI water was again used to flush away “free” Au NPs, while the attached Au NPs left on the ssDNA-modified

sensing film. In this case, graphene, ssDNA and Au NPs formed a sandwich structure on the Au film substrate, which resulted in a strong change in the overall SPR signal (Figure 3c). In a control test, Au nanoparticles were supplied under same conditions without the ssDNA adsorption step. However, we did not record any significant change of the phase signal (inset to Figure 3c), which evidenced the absence of any affinity between the positively charged nanoparticles and graphene-coated gold. Figure 3d summarizes the signal enhancement factors under different concentrations of ssDNA. One can see that the largest enhancement was obtained for ssDNA solutions with 100 aM, while higher concentrations (100 fM - 100 nM) led to slightly lower enhancement factors. Such decrease of enhancement under high concentration can be explained by the saturation of SPR signal due to a complete coverage of ssDNA within the light spot area (1mm × 1mm) of the sensing film. It should be noted that observed nanoparticle-based enhancement factors are in good agreement with our numerical analysis (Supporting Information Figure S3 and S4).

To summarize the obtained data, when used with Au amplification tags, the graphene-gold biosensing structure provided the detection limit of 1 aM (10^{-18} M) for 7.3kDa 24-mer ssDNA at a signal-to-noise ratio of 3:1, which is higher than the detection limit reported for not only current state-of-the-art graphene-based SPR biosensor (human IgG of 150 kDa, 0.5 nM, ref. 32) and Au NP-enhanced phase-sensitive SPR techniques (TNF-α of 17 kDa, 0.03 pM, ref. 23), but also gold nanorod-enhanced localized SPR sensors (streptavidin of 53 kDa, 10 nM, ref. 3) and even nanomechanical biosensors (25-mer ssDNA of 7.6 kDa, 500 aM, ref. 33). The recorded sensitivity evidence a huge potential of the graphene-gold metasurface architectures for detecting many other aromatic ring structure biomolecules (toxins, vitamins, cancer biomarkers, etc.) for which conventional SPR is not sensitive enough. We envision that a proper functionalization of Au nanoparticles by complementary counterparts of targeted biomolecules will further improve the bio-selectivity of our engineered sensing configuration.[34]

In summary, the designed novel graphene-gold metasurface-based biosensing architectures, which make possible extreme phase singularities due to a strong field enhancement on the graphene/gold interface. Profiting from these singularities, we recorded 4-times increase of sensitivity compared to phase-sensitive SPR and another order of magnitude gain of sensitivity by employing nanoparticle-based enhancement of phase signals. One of huge advantages of the proposed architectures over conventional plasmonic biosensing consists in the possibility of involvement of strong pi-stacking forces in the development of functionalization strategies using many aromatic structure biomolecules (helical peptides, proteins, ssDNA etc.). For the conventional SPR detection using plain gold film, it is generally required to functionalize the gold sensing surface with capture molecules to enhance the adsorption efficiency before performing any measurement for detecting the targeted samples. For our sensing experiments here that uses graphene-coated film, we could achieve directly label-free ssDNA detection through the pi-stacking interaction between graphene and ssDNA without the need of any modification steps for preparing “activated“ sensing film. As an example, we illustrated at least 3-orders gain in sensitivity by using a model of ssDNA adsorption on graphene-gold metasurface. Our system was subjected to continue evaluation for six months for determining the setup stability and showed same reproducibility for all the repeated experiments. It is worth noting that our graphene sensing substrate is fabricated based on pristine graphene layers, which are known to have better optical and electronic properties in comparison to the layers obtained by self-assembly of graphene oxides (GOs). The higher electron transfer rate and higher optical transparency of our pristine graphene sensing substrate also lead to a much stronger plasmon enhancement effect that resulted in extreme singularities in phase of reflected light of the metasurface. Further studies will be required to evaluate the designed system for detecting a series of aromatic ring structure biomolecules ranging from vitamins to helical peptides. As shown in Supporting Information Figure S10 and S11, proteins adsorbed on the graphene surface through pi

stacking interactions still maintain their biological activities such as catalytic activity of the enzyme. We envision that the reported sensing configuration will play an important role in designing future high-throughput multi-sensing platforms for clinical diagnostics of human diseases such as cancers. For example, our system will be able to sense cysteine-rich intestinal protein (CRIP) at aM level, a 8.5-kDa protein that has been identified as an useful biomarker for detecting early stages of human breast cancer, cervical cancer and pancreatic cancer.[35]

Supporting Information
Supporting Information is available from the Wiley Online Library or from the author.

Acknowledgement
This work was supported by the Singapore Ministry of Education (Grants Tier 2 MOE2010-T2-2-010 (M4020020.040 ARC2/11) and Tier 1 M4010360.040 RG29/10), NTU-NHG Innovation Collaboration Grant (No. M4061202.040), A*STAR Science and Engineering Research Council (No. M4070176.040) and School of Electrical and Electronic Engineering at NTU.

Reference

[1] S. Zeng, D. Baillargeat, H.-P. Ho, K.-T. Yong, *Chem. Soc. Rev.* **2014**, *43*, 3426.

[2] A. V. Kabashin, P. Evans, S. Pastkovsky, W. Hendren, G. A. Wurtz, R. Atkinson, R. Pollard, V. A. Podolskiy, A. V. Zayats, *Nature Mater.* **2009**, *8*, 867.

[3] P. Zijlstra, P. M. R. Paulo, M. Orrit, *Nature Nanotech.* **2012**, *7*, 379.

[4] B. Liedberg, C. Nylander, I. Lundstrom, *Sensors Actuators B* **1983**, *4*, 299.

[5] J. Homola, *Surface Plasmon Resonance Based Sensors*, Springer, **2006**.

[6] J. N. Anker, W. P. Hall, O. Lyandres, N. C. Shah, J. Zhao, R. P. Van Duyne, *Nature Mater.* **2008**, *7*, 442.

[7] V. G. Kravets, F. Schedin, R. Jalil, L. Britnell, R. V. Gorbachev, D. Ansell, B. Thackray, K. S. Novoselov, A. K. Geim, A. V. Kabashin, A. N. Grigorenko, *Nature Mater.* **2013**, *12*, 304.

[8] P. N. Prasad, *Introduction Introduction to Nanomedicine and Nanobioengineering*. John Wiley & Sons, **2012**.

[9] M. A. Cooper, *Nature Rev. Drug Discov.* **2002**, *1*, 515.

[10] A. V. Kabashin, P. I. Nikitin, *Quantum Electron.* **1997**, *27*, 653.

[11] H. P. Ho, W. W. Lam, *Sensors Actuators B* **2003**, *96*, 554.

[12] Y. Huang, H. P. Ho, S. K. Kong, A. V. Kabashin, *Ann. Phys. (Berlin)* **2012**, *524*, 637.

[13] A. V. Kabashin, S. Patskovsky, A. N. Grigorenko, *Opt. Express* **2009**, *17*, 21191.

[14] N. I. Zheludev, Y. S. Kivshar, *Nature Mater.* **2012**, *11*, 917.

[15] A. N. Grigorenko, M. Polini, K. S. Novoselov, *Nature Photon.* **2012**, *6*, 749.

[16] Q. L. Bao, K. P. Loh, *ACS Nano* **2012**, *6*, 3677.

[17] H. Yan, T. Low, F. Guinea, F. Xia, P. Avouris, *Nano Lett.* **2014**, *14*, 4581.

[18] R. Verma, B. D. Gupta, R. Jha, *Sensors Actuators B* **2011**, *160*, 623.

[19] P. Wang, O. Liang, W. Zhang, T. Schroeder, Y.-H. Xie, *Adv. Mater.* **2013**, *25*, 4918.

[20] L. Wu, H. S. Chu, W. S. Koh, E. P. Li, *Opt. Express* **2010**, *18*, 14395.

[21] B. Song, D. Li, W. P. Qi, M. Elstner, C. H. Fan, H. P. Fang, *Chem. Phy. Chem.* **2010**, *11*, 585.

[22] S. Akca, A. Foroughi, D. Frochtzwajg, H. W. C. Postma, *Plos One* **2011**, *6*, e18442.

[23] W. C. Law, K. T. Yong, A. Baev, P. N. Prasad, *ACS Nano* **2011**, *5*, 4858.

[24] M. J. Kwon, J. Lee, A. W. Wark, H. J. Lee, *Anal. Chem.* **2012**, *84*, 1702.

[25] A. V. Kildishev, A. Boltasseva, V. M. Shalaev, *Science* **2013**, *339*, 1232009.

[26] N. Yu, F. Capasso, *Nature Mater.* **2014**, *13*, 139.

[27] I. Pockrand, *Surf. Sci.* **1978**, *72*, 577.

[28] P. K. Jain, K. S. Lee, I. H. El-Sayed, M. A. El-Sayed, *J. Phys. Chem. B* **2006**, *110*, 7238.

[29] G. Giovannetti, P. A. Khomyakov, G. Brocks, V. M. Karpan, J. van den Brink, P. J. Kelly, *Phys. Rev. Lett.* **2008**, *101*, 026803.

[30] R. R. Nair, P. Blake, A. N. Grigorenko, K. S. Novoselov, T. J. Booth, T. Stauber, N. M. R. Peres, A. K. Geim, *Science* **2008**, *320*, 1308.

[31] S. H. Choi, Y. L. Kim, K. M. Byun, *Opt. Express* **2011**, *19*, 458.

[32] H. Zhang, Y. Sun, S. Gao, J. Zhang, H. Zhang, D. Song, *Small* **2013**, *9*, 2537.

[33] Y. Lu, S. Peng, D. Luo, A. Lal, *Nature Commun.* **2011**, *2*, 578.

[34] S. Zeng, K.-T. Yong, I. Roy, X.-Q. Dinh, X. Yu, F. Luan, *Plasmonics* **2011**, *6*, 491.

[35] J. Hao, A. W. R. Serohijos, G. Newton, G. Tassone, Z. Wang, D. C. Sgroi, N. V. Dokholyan, J. P. Basilion, *Plos Comput. Biol.* **2008**, *4*, e1000138.

Received: April 13, 2015
Revised: August 3, 2015
Published online:

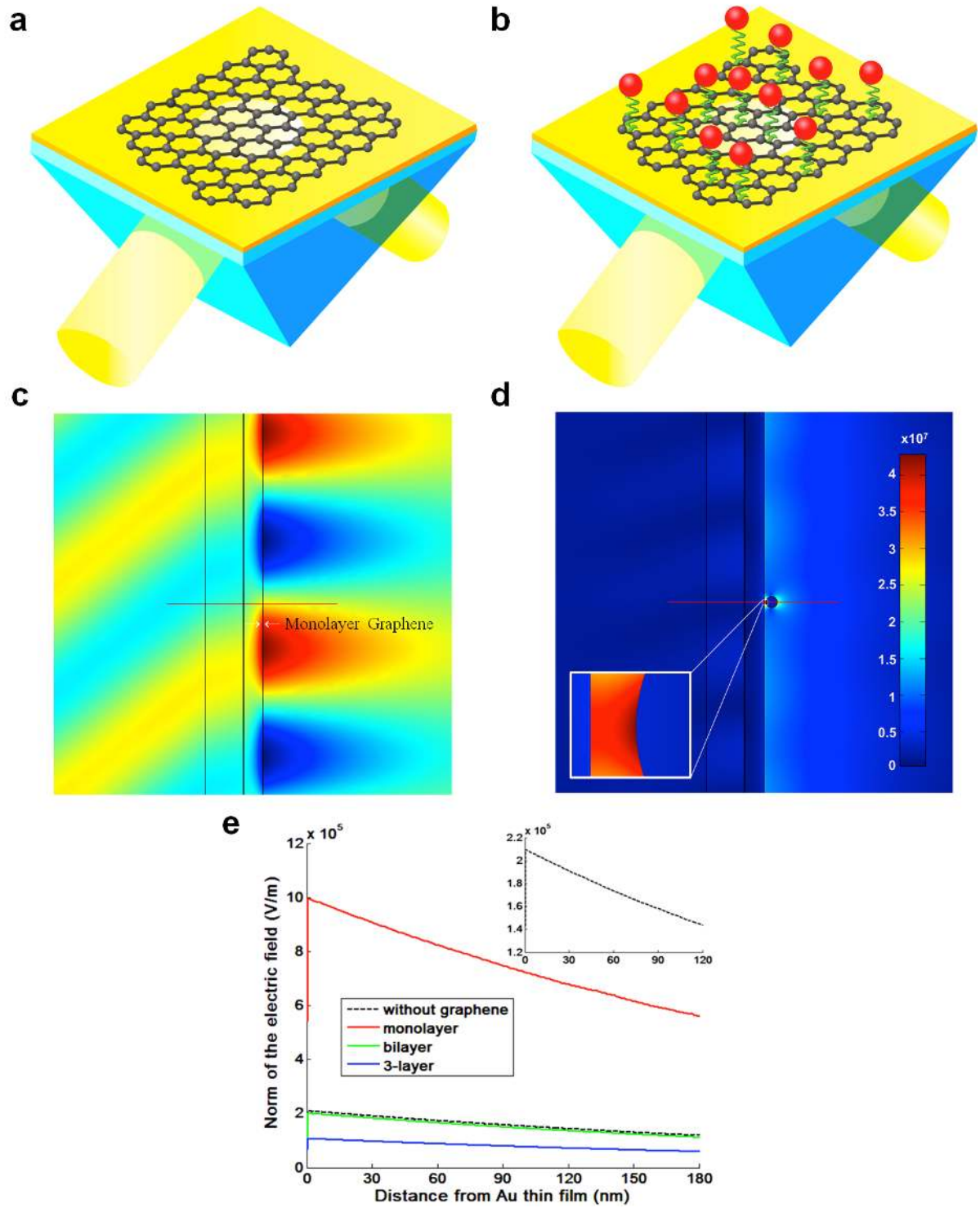

Figure 1. Designs of Graphene-gold metasurface architectures. (a) Basic architecture with a layer of graphene deposited on the gold surface. To excite Surface Plasmon Polariton over the Graphene-gold interface, a light beam is typically passed through a glass prism and reflected from a 50-nm gold film deposited on one of its facets; (b) Advanced nanoparticle-enhance architecture with the employment of Au nanoparticles as SPR amplification tags; (c) FEA simulations of resonant monolayer graphene-coated Au sensing film: Electric field in y component, showing angle of incident light ~52° and clear evanescent field at the sensing interface; (d) FEA simulations of resonant spherical-Au NP coupling to the monolayer graphene-coated Au sensing film: Norm of the electric filed with Au NP (diameter is 30nm,

distance from the sensing film is 5nm); (e) Cross-section plots for total electric fields along y=0 with different number of graphene layers *L*.

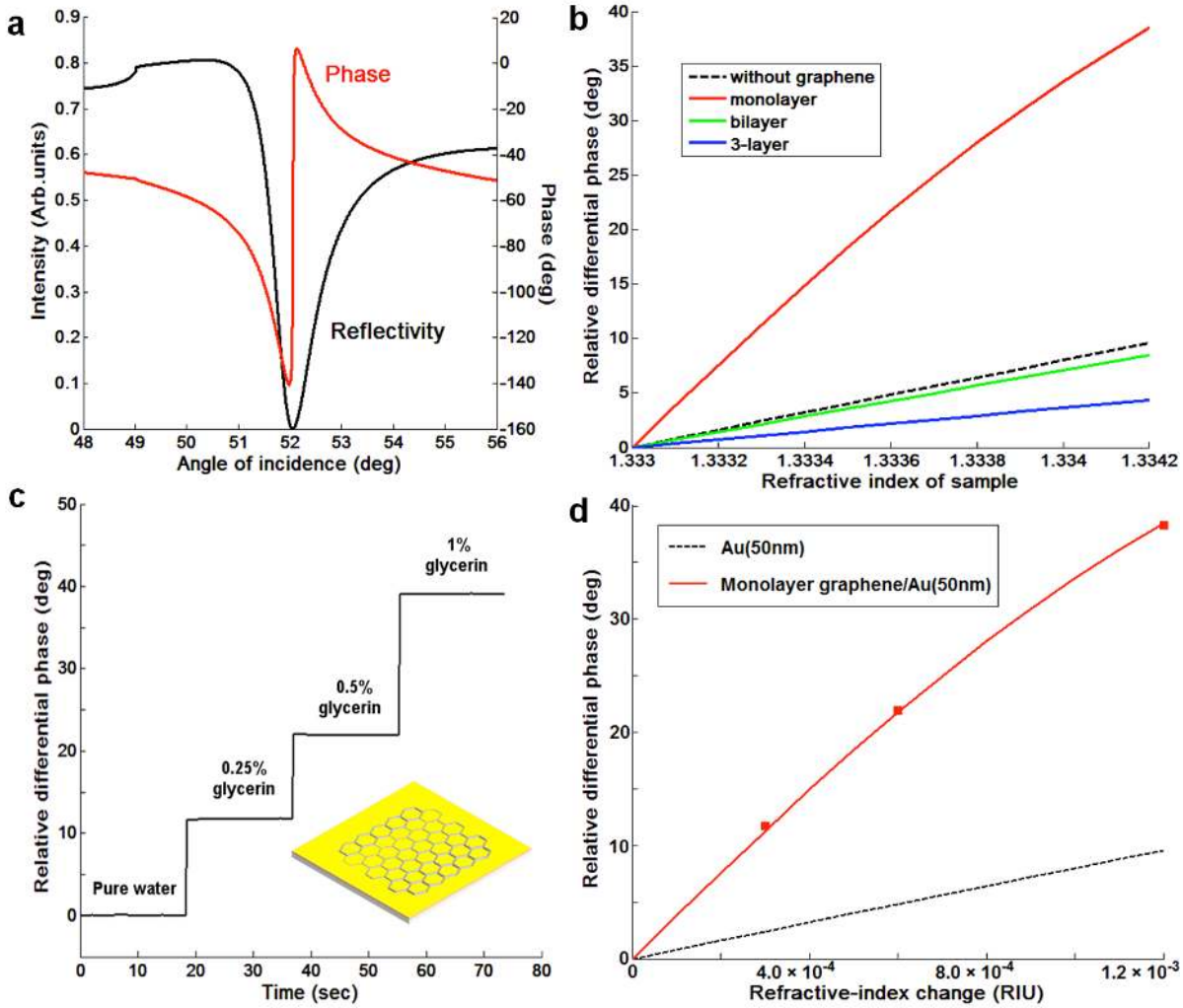

Figure 2. Assessment of phase sensitivity of graphene-gold metamaterial to refractive index variations. (a) Calculated reflectivity (black) and phase (red) of light as functions of the angle of light incidence of the gold/graphene interface, corresponding to maximum probing field. Phase experiences a sharp singularity in the minimum of SPR curve; (b) Response of phase due to the adsorption of biomolecules with different number of graphene layers *L*; (c) Real-time differential phase measurement for various weight ratios of glycerin in water using monolayer graphene-coated Au thin film as sensing substrate. The baseline was measured after flowing deionized (DI) water onto the sensor surface; (d) Comparison of calibration curves for graphene-coated gold film and pure Au film substrates under changes of the refractive index in the environment. All lines in the figure are theoretical analyses. The square symbols correspond to experimental measurements in Figure 2c.

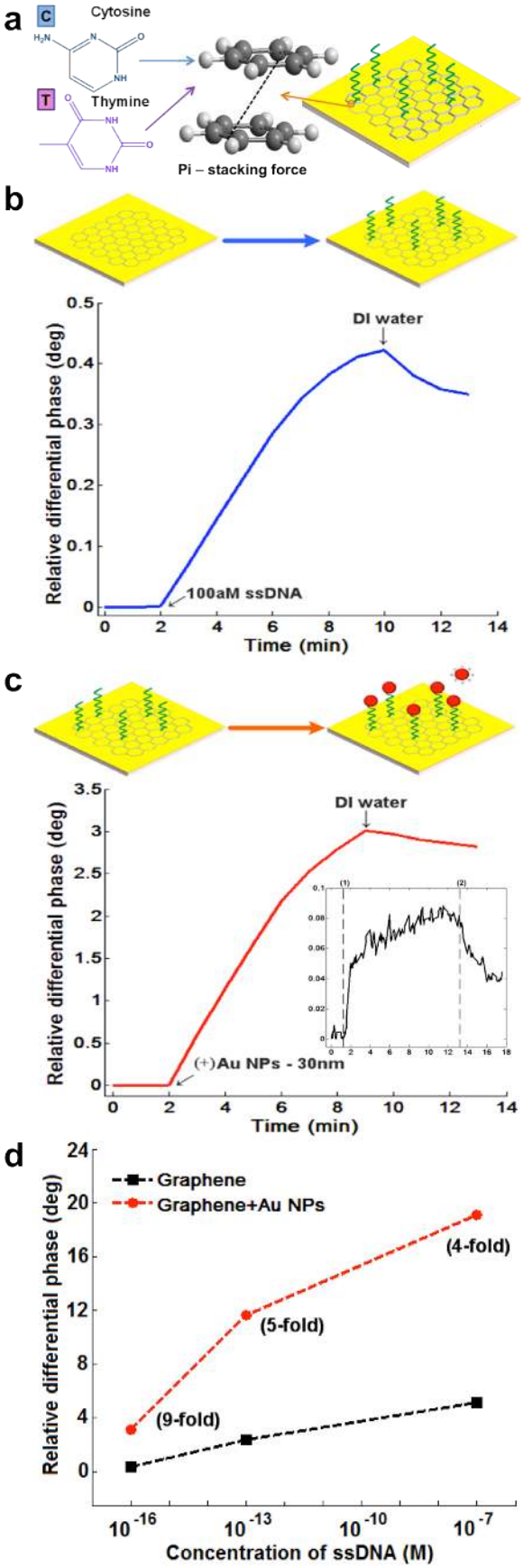

Figure 3. Detection of low-concentration ssDNA by biosensor employing graphene-gold metasurface architectures. (a) Schematics of binding ssDNA to monolayer graphene-coated

Au thin film by pi-stacking interaction; (b) and (c) are response curves obtained after flowing solutions of ssDNA with concentration of 100 aM (b) and positive-charged Au NPs with 30nm in diameter (OD=1.0) (c), followed by DI water. The baselines were measured after flowing deionized (DI) water (b) and binding of 100 aM ssDNA (c) onto the sensor surface; The inset in (c) shows the absence of any unspecific binding between positive-charged Au NPs and bare monolayer graphene-coated sensing film while injecting solutions of positive-charged Au NPs with 30nm diameter (OD=1.0) (1) and DI water (2); (d) Response and magnitude of enhancement (in the bracket) obtained with (●) and without (■) exposing the monolayer graphene-coated sensing film to positive-charged Au NPs after ssDNA.

S2_Definition of Metasurface

(i) The definition of "metasurface" from the paper recently published in Science, entitled "Planar Photonics with Metasurfaces" [*Kildishev et al., Science 339, 1232009 (2013), cited by more than 260 times*] describes that "A metasurface structured on the subwavelength scale in the lateral directions can be deterministic (i.e., periodic and aperiodic) or random."

(ii) According to another review paper published in Nature Materials entitled "Flat optics with designer metasurfaces" [*Yu et al., Nat. Mater. 13, 139 (2014), cited by more than 190 times*], metasurfaces can be made of optically thin films. Graphene layers are known as optically thin films [*Nair et al., Science 320, 1308 (2008), cited by more than 3000 times*]. In the Section of "Metasurfaces based on thin films" from Ref. [*Yu et al., Nat. Mater. 13, 139 (2014)*], the authors have clearly stated that "By properly choosing the materials of the film and the substrate, we can control the phase that light experiences reflecting at the interface between air and the film and at the interface between the film and the substrate, making it possible to engineer the phasor diagram or the reflection spectrum. In this sense, the thin-film/substrate structure can be regarded as a metamaterial with controllable complex refractive indices." For our proposed graphene-gold metasurface structure which uses complex refractive indices, we have obtained the optimum parameters to achieve the sharp phase jump at the SPR resonance angle and strong electric field enhancement that previously cannot be reached based on conventional Au substrates. In addition, the graphene-gold biosensing structure provided the detection limit of 1 aM (10^{-18} M) for 7.3kDa 24-mer ssDNA which is much higher than the detection limit reported for not only current state-of-the-art graphene-based SPR biosensor (human IgG of 150 kDa, 0.5 nM) and Au NP-enhanced phase-sensitive SPR techniques (TNF-α of 17 kDa, 0.03 pM), but also gold nanorod-enhanced localized SPR sensors (streptavidin of 53 kDa, 10 nM) and even nanomechanical biosensors (25-mer ssDNA of 7.6

kDa, 500 aM) [*Zhang et al., Small 9, 2537 (2013), Law et al., ACS Nano 5, 4858 (2011), Zijlstra et al., Nat. Nanotech. 7, 379 (2012) and Lu et al., Nat. Commun. 2, 578 (2011)*].

Supporting Information

Graphene-gold Metasurface Architectures for Ultrasensitive Plasmonic Biosensing

*Shuwen Zeng, Kandammathe Valiyaveedu Sreekanth, Jingzhi Shang, Ting Yu, Chih-Kuang Chen, Feng Yin, Dominique Baillargeat, Philippe Coquet, Ho-Pui Ho, Andrei V. Kabashin and Ken-Tye Yong**

Contents

1.Theoretical modeling

1.1. Optimization of the number of graphene layers coated on the plasmonic sensing film

The number of graphene layers used in our proposed graphene-gold metasurface enhanced enhanced plasmonic sensing configuration was studied and optimized by using two numerical analysis methods: (i) Transfer-matrix method (TMM) and (ii) Finite element analysis (COMSOL Multiphysics 3.5). The results from both approaches indicated that monolayer graphene induced the largest field enhancement and thus led to the highest phase sensitivity to the refractive-index change of sensing medium.

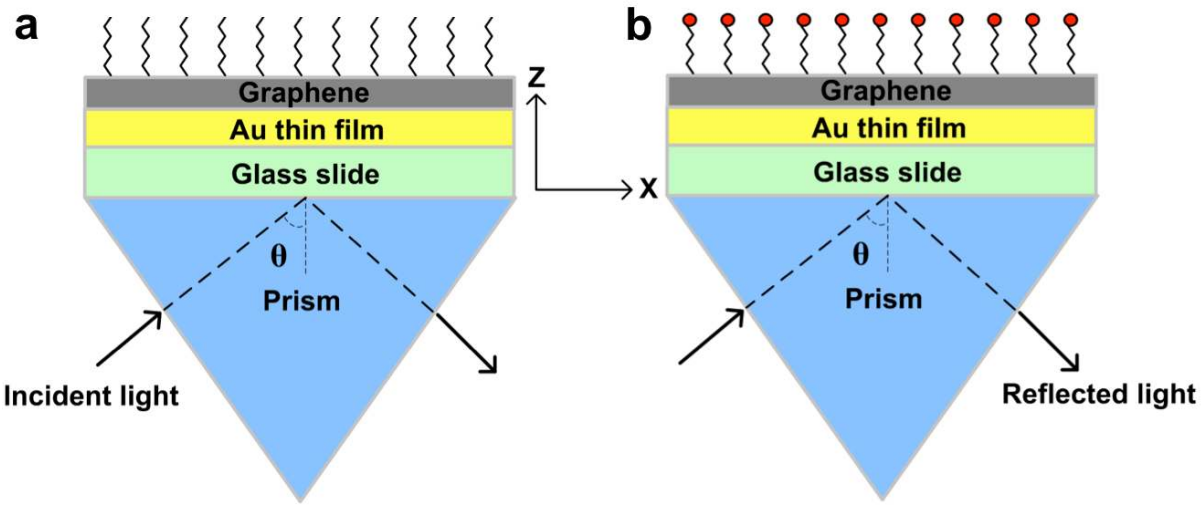

Figure S1. Two biosensing architectures based on graphene-gold metasurface. (a) Basic architecture with a layer of graphene deposited on gold; (b) Au nanoparticle-enhanced architecture with additionl use of Au nanoparticles as signal amplification tags.

1.1.1. Transfer-matrix method (TMM)

Figure S1 shows schematically two possible biosensing architectures employing graphene-gold metasurfaces. A BK7 glass slide coated with 50nm-thick Au thin film was attached to the base of SF11 prism. The graphene layers transferred on top of Au thin film were placed in

contact with sensing medium containing biomolecules to be detected. According to the conditions for SPR excitation of this Kretchmann structure [1], wave vector of the incident light projected in the x direction k_x, should be matched with that of the surface plasmon oscillations k_{sp}:

$$k_x = k_{sp} \quad \text{where } k_x = k_0 n_{prism} \sin\theta_{inc} \tag{1}$$

Here k_0 is the wave vector of the incident light in free space. A 785nm laser diode was used for illuminating the sensing substrate. The refractive indices at λ =785nm of SF11 prism, BK7 glass slide and Au thin film were set to be n_1 = 1.76552, n_2 = 1.51108 and n_3 = 0.14891 + i4.7830, respectively [2]. Since the thickness of the glass slide does not affect SPR curves [3], we set this parameter to be d_2 = 100nm in our calculation for simplification. For graphene layers, the complex refractive index was given by n_4 = 2.90 + i1.50 at 785nm [4]. The thickness of monolayer graphene (MG) is 0.34nm, and hence multilayer of graphene owns a thickness of $d_4 = L \times 0.34$nm, where L is the number of graphene layers.

By using the transfer-matrix method (TMM), the total reflection coefficient (r_p) for p-polarization light in our N-layer SPR sensing system is [5]:

$$r_p = \frac{(M_{11} + M_{12}q_N)q_1 - (M_{21} + M_{22}q_N)}{(M_{11} + M_{12}q_N)q_1 + (M_{21} + M_{22}q_N)} \tag{2}$$

$$M = \prod_{k=2}^{N-1} M_k = \begin{bmatrix} M_{11} & M_{12} \\ M_{21} & M_{22} \end{bmatrix} \tag{3}$$

with

$$M_k = \begin{bmatrix} \cos\beta_k & -i\sin\beta_k / q_k \\ -iq_k \sin\beta_k & \cos\beta_k \end{bmatrix} \tag{4}$$

where

$$q_k = \left(\frac{\mu_k}{\varepsilon_k}\right)^{1/2} \cos\theta_k = \frac{\left(\varepsilon_k - n_1^2 \sin^2\theta_1\right)^{1/2}}{\varepsilon_k} \tag{5}$$

$$\beta_k = d_k \left(\frac{2\pi}{\lambda}\right)\left(\varepsilon_k - n_1^2 \sin^2\theta_1\right)^{1/2} \tag{6}$$

Here, ε_k and d_k represent the optical constant and thickness of *k*-th layer. λ and θ_1 are the wavelength of the incident light and angle of incidence as shown in Fig. S1. Finally, the phase of *p*-polarization ϕ_p is obtained as:

$$\phi_p = \arg\left(r_p\right) \tag{7}$$

For *s*-polarization light the above equations hold except:

$$q_k = \left(\frac{\varepsilon_k}{\mu_k}\right)^{1/2} \cos\theta_k = \left(\varepsilon_k - n_1^2 \sin^2\theta_1\right)^{1/2} \tag{8}$$

It is known that SPR only affects *p*-polarization light, *s*-polarization light can be served as a reference signal to eliminate environmental noises for improving the stability and accuracy of SPR sensors [6]. Thus, the differential phase change between *p*- and *s*- polarization is obtained as $\phi_d = |\phi_p - \phi_s|$.

Through the above mentioned *N*-layer model, we could directly observe the influences of graphene on the nature of SPR. Here, we assumed that when the adsorption of biomolecules occurred, the refractive index of sensing medium (n_5) increased from 1.333 to 1.335 in an interval of 0.0001, and hence the total refractive index change of sensing medium was $\Delta n_5 = 0.002$. As shown in Fig. 2b, the relative differential phase change between *p*- and *s*- polarization linearly increased with increasing refractive index of the sensing medium. More importantly, monolayer graphene (MG) - coated sensing film exhibited a much more significant phase change at the SPR resonance angle compared to that of without graphene layers. The slope of relative differential phase change was observed to be gradually reduced when the number of graphene layers was larger than 2. This occurred because of

the light energy loss due to over absorption of graphene layers, since each graphene layer absorbed 2.3% of transmitted light [7].

1.1.2. Finite element analysis (FEA)

Finite element analyses (FEA) were also used to verify the optimal number of graphene layers for enhanced SPR sensing. By numerically solving Maxwell's equations, we investigated the field intensity distributions on the SPR sensing system with different number of graphene layers coated on the sensing film as shown in Fig. 1c and 1e. All finite element analyses here were performed in two dimensions (2D). The solution space is 1.5 μm × 1.2 μm. The media in our modeling system starting from the left to right is: prism, glass slide, Au thin film, graphene layers and water, respectively. The red line in Fig. 1c indicates the cross-section range of the electric field. The center of the line is positioned in the middle of Au thin film (50nm in thickness). Figure 1c and 1e shows that under SPR excitation condition, clear evanescent fields were obtained. In addition, there were large field enhancements for monolayer graphene-coated sensing films.

For better illustration, we plotted out the enhancement factors for SPR signal change and maximum electric field as a function of the number of graphene layers (see Figure S2). The enhancement factors of SPR signal change and the maximum electric field agreed well and showed the same trend in optimizing the number of graphene layers.

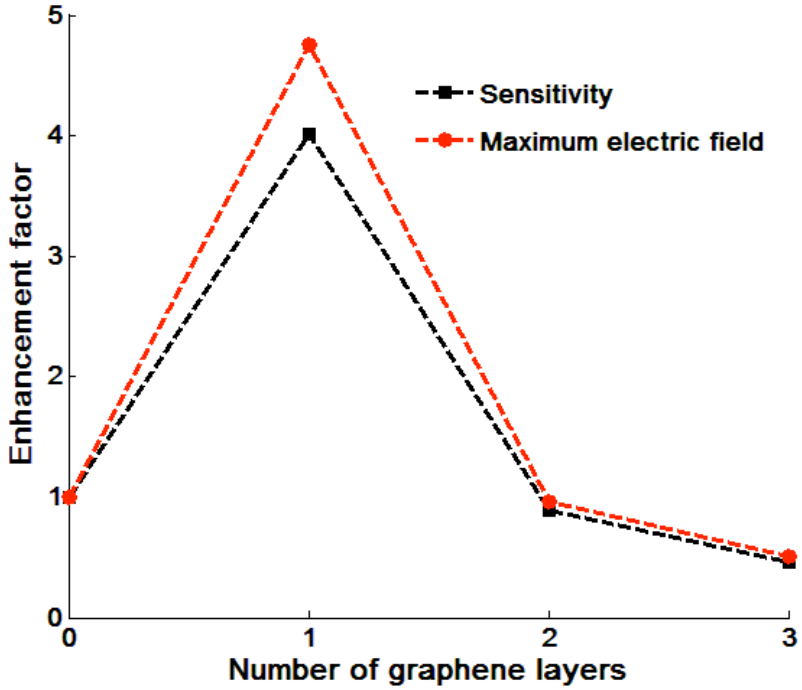

Figure S2. Enhancement factors as a function of number of graphene layers *L* for SPR signal change and maximum electric field, respectively.

1.2. Optimization of Au nanoparticle size for nanoparticle-enhanced sensing on graphene-gold metasurface

In our previous studies [8, 9], we found that coupling the localized SPR of metallic nanoparticles to the surface plasmon waves (SPW) of the sensing film could lead to a large field enhancement and thus improve the SPR sensitivity for detecting small molecules. Here, we fixed the number of graphene layers as one and used FEA method to study plasmon coupling effects in the SPR sensor with Au NPs in different diameters. We set the distance between Au NP and sensing film as 5 nm, which is the typical binding length of functional groups and targeted analytes [10]. The diameters of Au NPs that we focused here were ranging from 10 to 40 nm. It is worth noting that the scattering effects of Au NPs with large sizes (> 40 nm) are more pronounced against their absorption which will weaken the field enhancement according to Mie theory. Figure 1d and S3 show that with monolayer graphene (MG)-coated on the Au thin film, the electric field between Au NP of 30 nm and the sensing film was enhanced by more than 40 times in comparison to that of without Au NP. The

largest enhanced electric field that occurred with coupling of 30 nm Au NP was attributed to the highest absorption efficiency and lowest scattering efficiency of the 30 nm Au nanoparticle when they are coupled to the graphene coated-Au thin film. Thus, we chose Au NPs with diameters of 30 nm as amplification tags coupling to MG-coated sensing film in the enhanced SPR sensing measurements for low-concentration ssDNA detection.

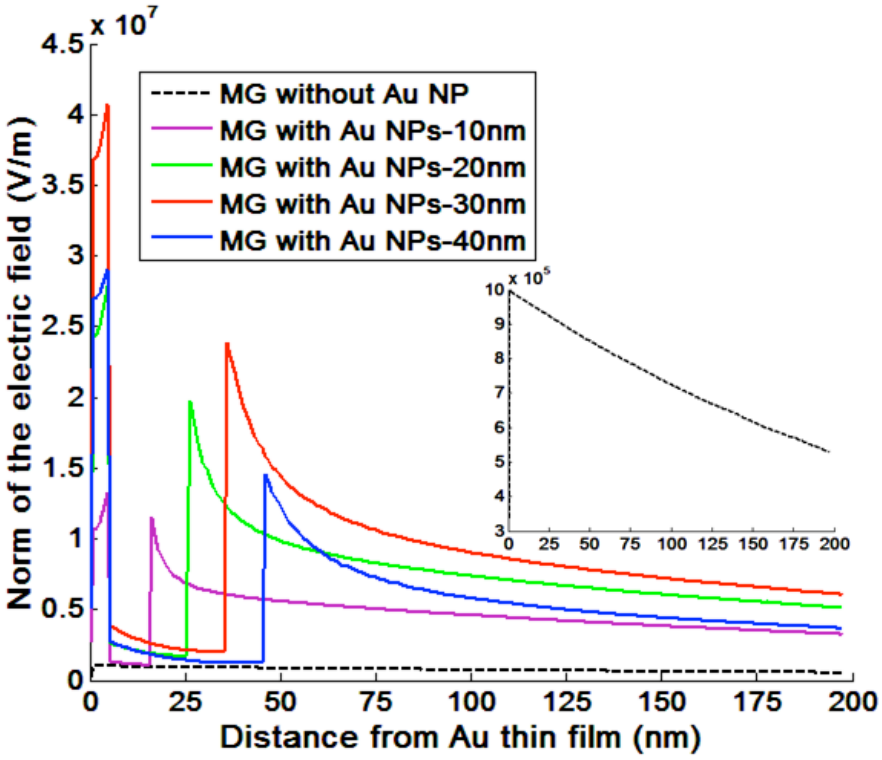

Figure S3. Cross-section plots of total electric fields showing different diameters of Au NP resonant coupling to the sensing film coated with monolayer graphene. The electric fields for Au NP with diameter of 10nm, 20nm and 40nm are magnified by a factor of 10 for clarity.

Electric fields between Au NP and the sensing film without coating graphene were also studied. It was shown that in the case of no graphene was coated on the Au thin film, the electric fields between Au NP and the sensing film were enhanced as well compared to those of without Au NP (see Figure S4). The maximum field enhancement was achieved using Au NP with 40 nm in diameter coupling to bare Au thin film, yet it was still 3 times lower than that of coupling with graphene-coated Au thin film. These results indicated that our proposed graphene-Au NPs enhanced

SPR sensor owned a much higher sensitivity than that of pure graphene-enhanced SPR and Au NP-enhanced SPR detection methods.

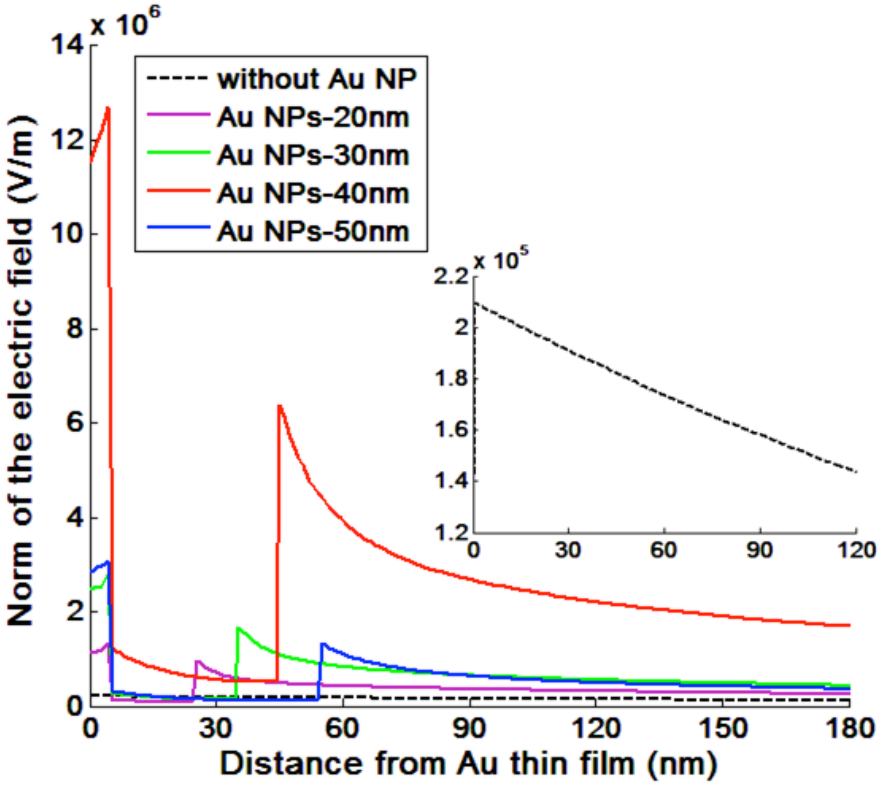

Figure S4. Cross-section plots of total electric fields showing different diameters of Au NP resonant coupling to the sensing film coated without graphene. The electric fields for Au NP with diameter of 20nm, 30nm and 50nm are magnified by a factor of 10 for clarity.

According to the calculation results based on Mie theory for Au NPs with diameters ranging from 20 nm to 80 nm, the Au NP with a diameter of 40 nm has the highest absorption efficiency and lowest scattering efficiency [11]. For the SPR excitation, higher absorption efficiency is required since more incident light energy can be successfully transferred to the resonance energy of the SPR waves. For a fixed incident light energy, the larger the intensity of the excited electric field, the higher the transfer rate. From Figure S4, we can see that the field enhancements possess a peak value when 40 nm Au NPs were coupled to the pure Au thin film. These results demonstrate that the interaction trend between absorption efficiency

and the Au NP diameter has not been modified by the proximity of the Au NPs to the pure Au thin film. On the other hand, when 30 nm Au NPs were coupled to the graphene coated-Au thin film (see Fig. S3), a peak value was observed from the field enhancement plot. The smaller optimum Au NP diameter means that the interaction trend between the absorption efficiency and the Au NP diameter has been slightly modified by the proximity of the Au NPs to graphene coated-Au thin film due to the large difference in the dielectric constants between Au and graphene.

2. Experimental

2.1. Materials

Glycerin (≥ 99%) was purchased from Sigma-Aldrich. Desalted 24-mer single-stranded DNA sequence (5'-CTT CTG TCT TGA TGT TTG TCA AAC-3') with concentration of 100μM was purchased from AITbiotech. Positive-charged spherical gold nanoparticles (OD=1.0) with diameters of 30nm and zeta potential of 20mV were purchased from Nanopartz Accurate. The size variance was less than 1%. All chemicals were used as received without further purification. Ultrapure deionized (DI) water was obtained by Spectra-Teknik water purification system. Glass slides coated with 50nm of gold film over 2.5nm Ti adhesion layer were purchased from Platypus.

2.2. Preparation of monolayer graphene-coated Au thin film

Monolayer graphene was grown on high-purity (99.99%) copper foil by use of low-pressure chemical vapor deposition (Easytube 3000, Firstnano). 50 sccm H_2 and 200 sccm methane were introduced as gas sources. The growth chamber was held at 1000 °C under a low pressure of 2 Torr. After that, the graphene was transferred from the copper substrate to the

Au thin film as described in our previous reports [12, 13]. The same batch graphene was also transferred onto commercial SiO_2/Si substrate to check the sample quality by Raman spectroscopy.

A 532nm Renishaw Raman system with a 2400 lines/mm grating was employed to measure Raman spectra of the prepared graphene. A typical Raman spectrum is shown in Fig. S5. It is visible that the peak intensity ratio of G to 2D is ~ 0.5. The weak disorder-induced D band indicated the high crystal quality of this sample. To check the uniformity, the Raman data from 10 random sampling regions on the CVD-grown monolayer graphene on SiO_2/Si have been collected as shown in Fig. S6. The positions of G and 2D bands were located at 1589 ± 2 and 2685 ± 2 cm^{-1}, respectively. The corresponding FWHMs of two bands were 18 ± 3 and 36 ± 3 cm^{-1}, respectively. These features of Raman bands agreed well with the characteristics of the monolayer graphene grown by other groups [14, 15].

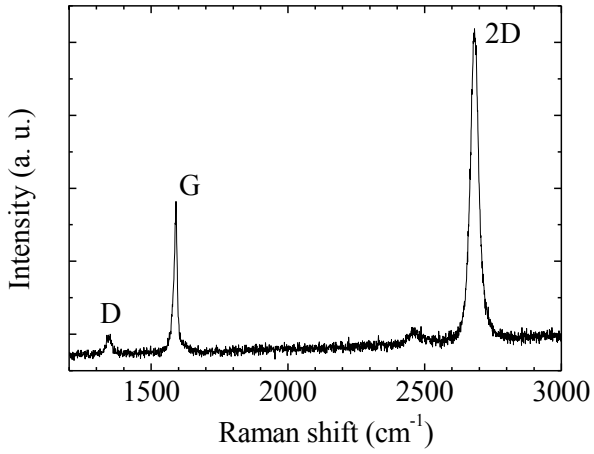

Figure S5. Raman spectrum of the CVD-grown monolayer graphene.

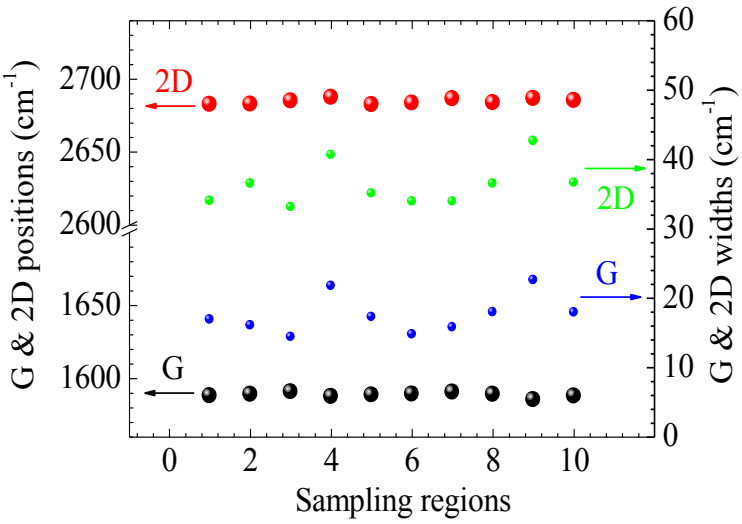

Figure S6. Peak positions and widths of G and 2D bands from 10 random sampling regions on the CVD-grown monolayer graphene.

2.3. Graphene-gold metasurface enhanced plasmonic sensing measurements

2.3.1. Plasmonic sensor

All the plasmonic sensing measurements were performed using a home-built differential phase-sensitive SPR sensor, as shown schematically in Fig. S7. We used an 80-mW 785 nm laser diode as the excitation light source. The incident light beam with spot size ~1mm was 45° linearly polarized for both *p*- and *s*-polarizations. The incident angle was fixed at ~52°. The SPR sensor was based on a Mach–Zehnder interferometric scheme in order to improve its stability. The sensor head was in the signal beam. It consisted of an equilateral SF11 prism (Edmund optics) and a flow chamber that allowed the sample solutions to interact with the sensing film. The fabricated monolayer graphene-coated Au sensing film was attached to the prism through optical matching oil (Cargille labs). A syringe pump was used to flow sample solutions into the flow chamber with a flow rate of ~5 microliters per second. In the reference beam, a piezoelectric transducer (PZT) mirror was driven by sawtooth wave signals

oscillating at 86 Hz to generate optical path differences and obtain complete sine waves for both *p*- and *s*- polarizations. A Wollaston prism was used to separate the final interfered light beam into *p*- and *s*- polarized light. Real-time data of the two polarized light beams were received by a two-channel photodetector and collected through a data acquisition card (NI PCI-6115) using a Labview program. A point-wise arcsine algorithm [16] was used to extract the phase difference between *p*- and *s*- polarized light after low-pass filtering.

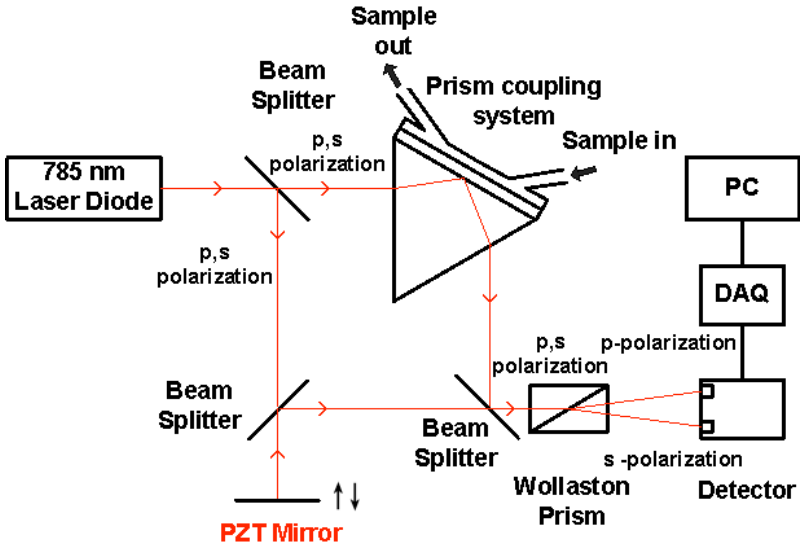

Figure S7. Schematic diagram of the differential phase-sensitive SPR sensor based on a modified interferometric configuration.

2.3.2. Calibrations using MG-coated and bare Au sensing films

In the calibration processes, we flowed glycerin solutions with different weight ratios to the flow chambers through syringe pumps as introduced in section 2.3.1. The corresponding refractive index from pure DI water to 2.5% glycerin is measured to be from 1.333 to 1.336 by a refractometer. Figure 2c shows the sensing performances of monolayer graphene-coated Au thin film. For 0.5% glycerin, the refractive index change from pure water was 0.0006 refractive index units (RIU) and a phase change of 21.88° was achieved using the monolayer graphene-coated Au thin film. Stability of the sensing system was monitored for 10 min and

the fluctuation of differential phase was approximately 0.01°. These results agreed well with the theoretical calculations based on transfer matrix methods (see Figure 2d).

2.3.3. Low-concentration ssDNA detection

Solutions containing ssDNA with different concentrations ranging from 100 aM to 100 nM were respectively flowed into the SPR flow chambers and then interacted with the monolayer graphene-coated Au sensing films. Each time before injecting ssDNA solution, a calibration process as shown in Fig. 2c was carried out to check the quality of the MG-coated sensing substrate. The processes of binding of ssDNA to the surface of monolayer graphene-coated Au sensing film were monitored by our differential phase-sensitive SPR sensor. From Figure 3b, S8 and S9, one can see that obvious phase changes occurred upon the addition of ssDNA solution onto the sensor head. The system was left for about 8 min and then rinsed by DI water to confirm the binding of ssDNA to the surface of graphene-coated Au sensing film. Longer immersion times did not noticeably improve the signal change. To achieve a higher SPR sensitivity and further confirm the binding of ssDNA to the surface of graphene-coated sensing film, solutions containing positive-charged Au NPs with diameter of 30nm and unified optical density were then flowed onto the ssDNA-modified sensing substrate. Since the zeta potential of desalted ssDNA solution was negative, there would be strong electrostatic bindings occur when they encountered with the positive-charged Au NPs. After 8 min reaction time, DI water was running again to confirm the binding between Au NPs and the ssDNA-modified sensing film. In this case, the graphene, ssDNA and Au NPs formed sandwich structures. As described in the previous theoretical section, strong field enhancement between graphene and Au NPs directly related to the SPR sensitivity improvement. Response curves in Fig. 3c, S8 and S9 all show further enhancements of SPR sensing signals, which agree well with our prediction in section 1.2.

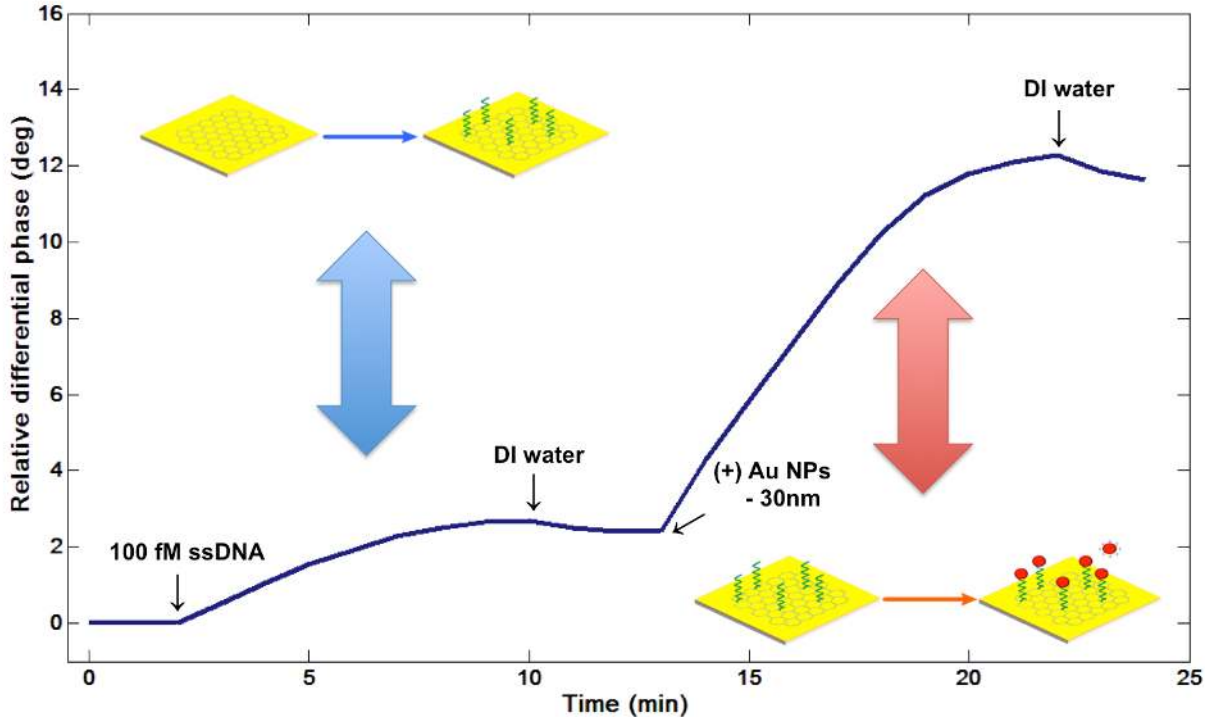

Figure S8. Response curve obtained after flowing solutions of ssDNA with concentration of 100 fM and positive-charged Au NPs with 30nm in diameter (OD=1.0), followed by deionized (DI) water. The baseline was measured after flowing DI water.

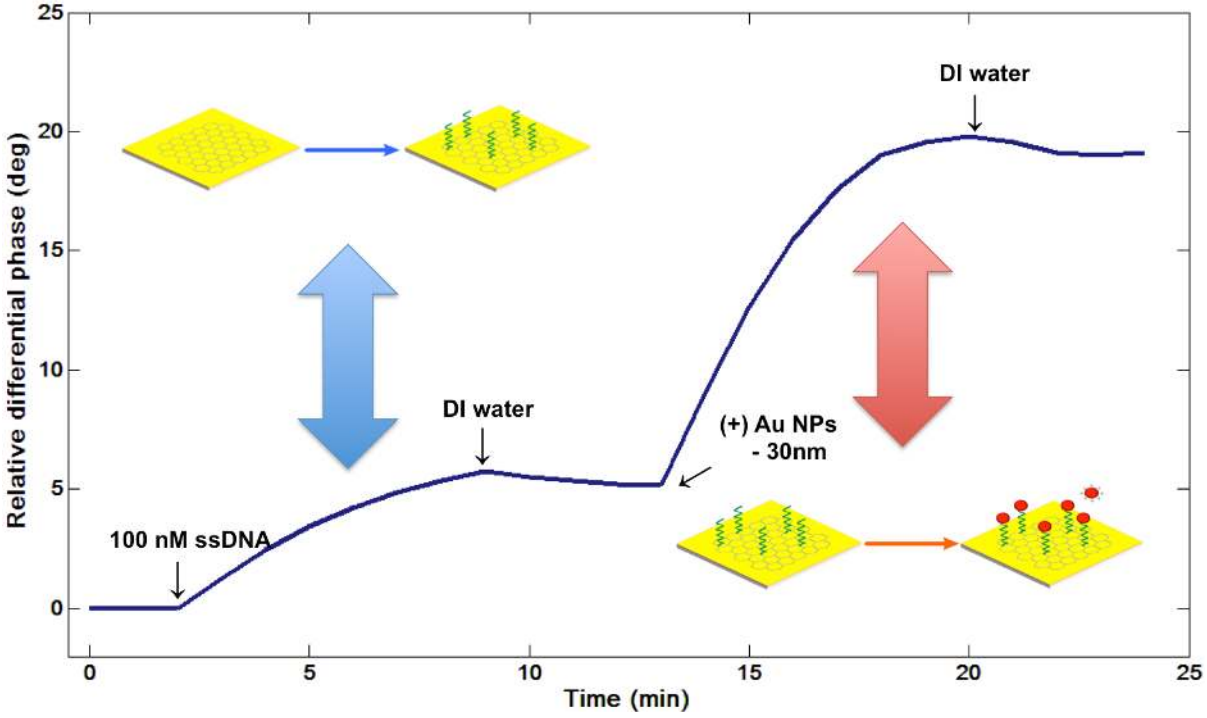

Figure S9. Response curves obtained after flowing solutions of ssDNA with concentration of 100 nM and positive-charged Au NPs with 30nm in diameter (OD=1.0), followed by deionized (DI) water. The baseline was measured after flowing DI water.

2.4. Evaluation of enzyme activity of protein adsorbed on graphene

Materials and methods

Peptides and recombinant proteins

H3K4me2 peptide was purchased from AnaSpec. Human LSD1 full-length cDNAs were obtained from Open Biosystems. Human LSD1 full-length cDNAs were fully sequenced and cloned into the pGEX-KG vector and expressed as the glutathione *S*-transferase (GST)-tagged fusion proteins in the *Escherichia coli* BL21 strain and affinity purified with Glutathione Sepharose-4B beads (GE Healthcare). Pristine graphene sheets obtained from CVD growth were dispersed in phosphate-buffered saline (PBS) solutions.

Antibodies and immunoprecipitation

LSD1 (ab17721) antibodies were obtained from Abcam. For immunoaffinity purification, recombinant LSD1 protein supernatant was incubated with Graphene or GST-Beads 2 hours at 4°C. Isolated Graphene-LSD1 or GST-Beads-LSD1 complexes were verified by Western blotting with LSD1 antibody.

In vitro demethylation assays

For a typical demethylation assay, 1 μg H3K4me2 substrate peptide was incubated individually with Graphene-LSD1or GST-Beads-LSD1 complexes at 30°C for 1 h. The reaction products were analyzed by mass spectrometry to separate the products (H3K4me1and H3K4) from the substrate (H3K4me2), as described in our previous study [17]. For mass-spectrometry analysis, 0.5 μL of the reaction mixture were equally mixed with 0.5 μL MALDI matrix (2mg/mL α-cyano-4-hydroxycinamic acid with 0.1% trifluoro-acetic acid)

and spotted onto the Opti-TOF^{TM} 384 Well Insert (Applied Biosystems) to allow solvent evaporation and peptides/matrix co-crystallization. The peptides were analyzed by 4800 Plus MALDI TOF/TOF tandem time-of-flight analyzer (Applied Biosystems). The conversion efficiency of the dimethylated (Me2) H3K4 peptide to mono- (Me1) and nonmethylated (Me0) H3K4 is calculated using the integrated product peak areas in MALDI-TOF and the following formula: Area (Me0)×2+ area (Me1)/[area (Me0)+area (Me1)+area (Me2)]×2.

Here, LSD1 (Lysine specific demethylase 1) was used as a protein model for the enzyme activity experiments. Firstly, we demonstrated the capability of pristine graphene for the adsorption of LSD1 through pi stacking interaction by using Western Blotting (see Figure S10). The recombinant GST-LSD1 protein was expressed in Escherichia coli BL21 strain and purified with Glutathione Sepharose-4B beads. Solution containing pristine graphene sheets was mixed with recombinant GST-LSD1 protein in 4°C for 1 hour, then washed by PBS buffer (135 mM NaCl, 2.7 mM KCl, 1.5 mM KH_2PO_4, and 8 mM K_2HPO_4, pH 7.2) 4 times. The graphene-GST-LSD1 complex was isolated by 2×SDS lysis buffer(100 mM Tris-Cl pH 6.8, 4% SDS, 12% Glycerol, 2% β-mercapitalethanol and 0.01% bromophenol blue) in 100°C for 30mins and LSD1 was verified by Western blotting with LSD1 antibody. GST beads that could specifically capture GST-LSD1 were used as positive control. Then, demethylase activity of the graphene-GST-LSD1 complex was tested (see Figure S11). For a typical demethylation assay, 1 μg H3K4me2 substrate peptide was incubated individually with graphene-LSD1 or GST-Beads-LSD1 complexes at 30°C for 1 h. The reaction products were analyzed by mass spectrometry to separate the products (H3K4me1and H3K4) from the substrate (H3K4me2). The results in Figure S10 and S11 showed that the LSD1 proteins have been successfully adsorbed to the graphene surface through pi stacking interactions and also maintained an effective enzyme activity. Thus, we believe that our graphene-gold

metasurface architectures could be not only employed in sensing DNA and oligonucleotides but also for the detection of other bioanalytes such as cancer biomarker and peptides.

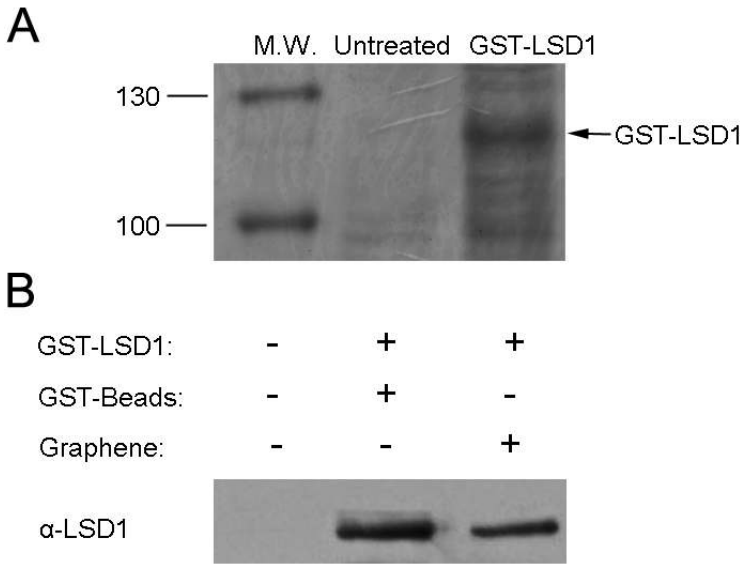

Figure S10. The identification of recombinant GST-LSD1 protein and the adsorption ability test of graphene. (A) Purified recombinant GST-LSD1 proteins were identified by SDS-Page gel and coomassie brilliant blue staining. Lanes M.W., molecular weight markers (in thousands). Untreated means no IPTG induced; (B) Recombinant GST-LSD1 protein supernatant was incubated with graphene or GST-Beads, followed by Western-Blotting.

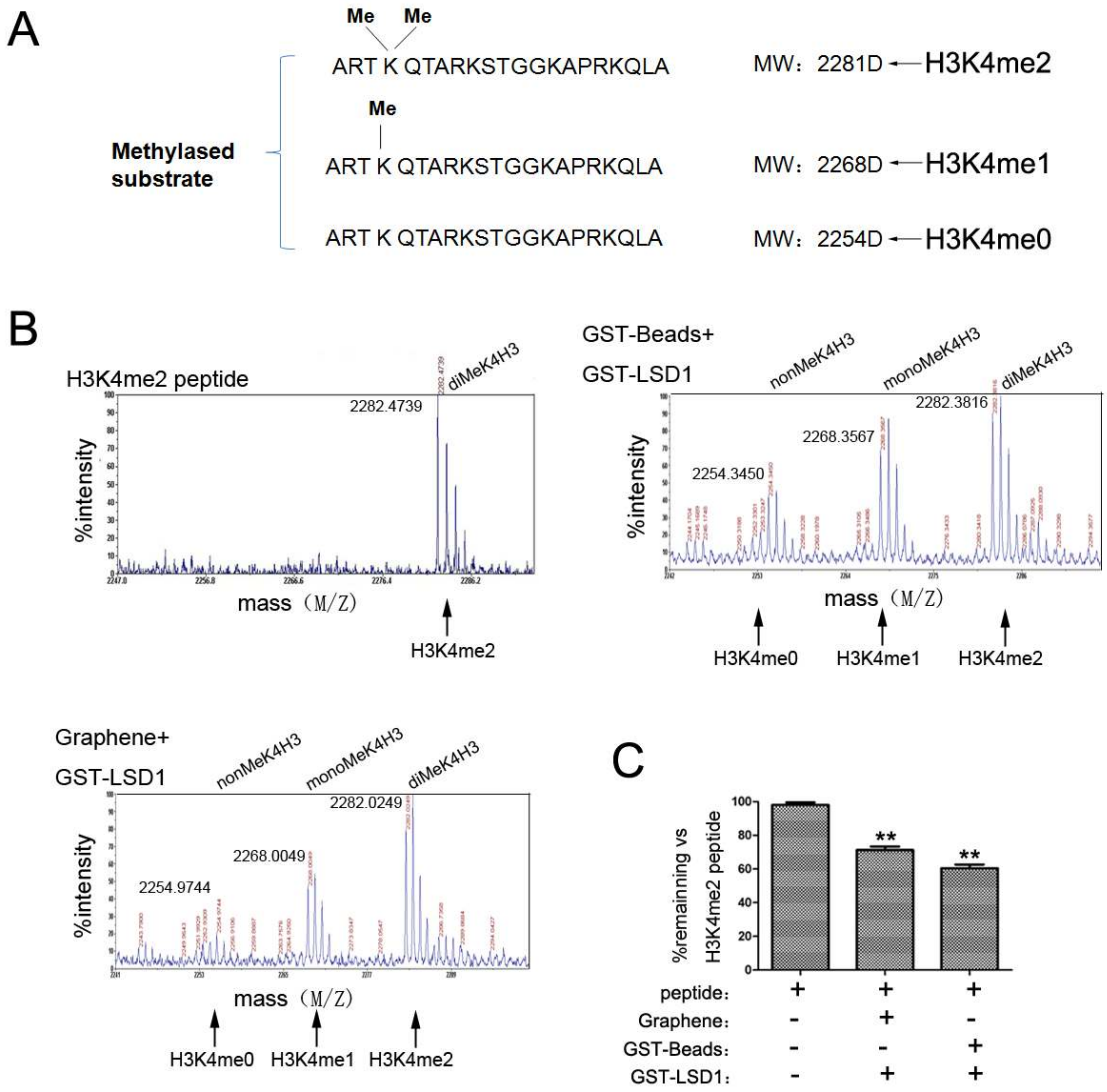

Figure S11. In vitro demethylation assay. (A) The sequences and molecular weight of methylated substrates. LSD1 could remove one or two methyl-group from H3K4me2 peptide. (B) LSD1 maintains its demethylated activity after the adsorption to graphene surface. The activity of LSD1 was tested by 800 Plus MALDI TOF/TOF tandem time-of-flight analyzer. GST-Beads could adsorb GST-LSD1 and keep its activity, as a positive control. (C) The peak areas of non-, mono- and di-methylated H3K4 were integrated to calculate the demethylated efficiency and the cartogram was made by the Graph-Pad Prism5 software. All experiments were conducted at least three times, and only the results of a representative experiment are shown. Error bars denote SEMs for duplicate samples. The statistical differences were analyzed by one-way ANOVA. **, $P < 0.01$.

References

1. Raether, H. *Surface Plasmons on Smooth and Rough Surfaces and on Gratings*. (Springer-Verlag, 1988).
2. Johnson, P.B. & Christy, R.W. Optical constants of the noble metals. *Phys. Rev. B* **6**, 4370-4379 (1972).
3. Xiao, C.D. & Sui, S.F. Characterization of surface plasmon resonance biosensor. *Sensors Actuators B* **66**, 174-177 (2000).
4. Weber, J.W., Calado, V.E. & van de Sanden, M.C.M. Optical constants of graphene measured by spectroscopic ellipsometry. *Appl. Phys. Lett.* **97,** 091904 (2010).
5. Hansen, W.N. Electric fields produced by the propagation of plane coherent electromagnetic radiation in a stratified medium. *J. Opt. Soc. Am.* **58**, 380-388 (1968).
6. Wu, S.Y., Ho, H.P., Law, W.C., Lin, C.L. & Kong, S.K. Highly sensitive differential phase-sensitive surface plasmon resonance biosensor based on the Mach-Zehnder configuration. *Opt. Lett.* **29**, 2378-2380 (2004).
7. Wu, L., Chu, H.S., Koh, W.S. & Li, E.P. Highly sensitive graphene biosensors based on surface plasmon resonance. *Opt. Express* **18**, 14395-14400 (2010).
8. Law, W.C., Yong, K.T., Baev, A. & Prasad, P.N. Sensitivity improved surface plasmon resonance biosensor for cancer biomarker detection based on plasmonic enhancement. *Acs Nano* **5**, 4858-4864 (2011).
9. Zeng, S. et al. Size dependence of Au NP-enhanced surface plasmon resonance based on differential phase measurement. *Sensors Actuators B* **176**, 1128-1133 (2013).
10. Law, W.C., Yong, K.T., Baev, A., Hu, R. & Prasad, P.N. Nanoparticle enhanced surface plasmon resonance biosensing: Application of gold nanorods. *Opt. Express* **17**, 19041-19046 (2009).
11. Jain, P.K., Lee, K.S., El-Sayed, I.H. & El-Sayed, M.A. Calculated absorption and scattering properties of gold nanoparticles of different size, shape, and composition: applications in biological imaging and biomedicine. *J. Phys. Chem. B* **110**, 7238-7248 (2006).
12. Sreekanth, K.V., Zeng, S.W., Shang, J.Z., Yong, K.T. & Yu, T. Excitation of surface electromagnetic waves in a graphene-based Bragg grating. *Sci. Rep.* **2** (2012).
13. Shang, J.Z., Yu, T., Lin, J.Y. & Gurzadyan, G.G. Ultrafast electron-optical phonon scattering and quasiparticle lifetime in CVD-grown graphene. *Acs Nano* **5**, 3278-3283 (2011).
14. Li, X.S. et al. Large-area synthesis of high-quality and uniform graphene films on copper foils. *Science* **324**, 1312-1314 (2009).
15. Kim, K.S. et al. Large-scale pattern growth of graphene films for stretchable transparent electrodes. *Nature* **457**, 706-710 (2009).
16. Ho, H.P., Law, W.C., Wu, S.Y., Lin, C.L. & Kong, S.K. Real-time optical biosensor based on differential phase measurement of surface plasmon resonance. *Biosens. Bioelectron.* **20**, 2177-2180 (2005).
17. Yin, F. et al. LSD1 Regulates Pluripotency of Embryonic Stem/Carcinoma Cells through Histone Deacetylase 1-Mediated Deacetylation of Histone H4 at Lysine 16. *Mol. Cell. Biol.* **34**, 158-179 (2014).

S2_Definition of Metasurface

(i) The definition of "metasurface" from the paper recently published in Science, entitled "Planar Photonics with Metasurfaces" [*Kildishev et al., Science 339, 1232009 (2013), cited by more than 260 times*] describes that "A metasurface structured on the subwavelength scale in the lateral directions can be deterministic (i.e., periodic and aperiodic) or random."

(ii) According to another review paper published in Nature Materials entitled "Flat optics with designer metasurfaces" [*Yu et al., Nat. Mater. 13, 139 (2014), cited by more than 190 times*], metasurfaces can be made of optically thin films. Graphene layers are known as optically thin films [*Nair et al., Science 320, 1308 (2008), cited by more than 3000 times*]. In the Section of "Metasurfaces based on thin films" from Ref. [*Yu et al., Nat. Mater. 13, 139 (2014)*], the authors have clearly stated that "By properly choosing the materials of the film and the substrate, we can control the phase that light experiences reflecting at the interface between air and the film and at the interface between the film and the substrate, making it possible to engineer the phasor diagram or the reflection spectrum. In this sense, the thin-film/substrate structure can be regarded as a metamaterial with controllable complex refractive indices." For our proposed graphene-gold metasurface structure which uses complex refractive indices, we have obtained the optimum parameters to achieve the sharp phase jump at the SPR resonance angle and strong electric field enhancement that previously cannot be reached based on conventional Au substrates. In addition, the graphene-gold biosensing structure provided the detection limit of 1 aM (10^{-18} M) for 7.3kDa 24-mer ssDNA which is much higher than the detection limit reported for not only current state-of-the-art graphene-based SPR biosensor (human IgG of 150 kDa, 0.5 nM) and Au NP-enhanced phase-sensitive SPR techniques (TNF-α of 17 kDa, 0.03 pM), but also gold nanorod-enhanced localized SPR sensors (streptavidin of 53 kDa, 10 nM) and even nanomechanical biosensors (25-mer ssDNA of 7.6 kDa, 500 aM) [*Zhang et al., Small 9, 2537 (2013), Law et*

al., ACS Nano 5, 4858 (2011), Zijlstra et al., Nat. Nanotech. 7, 379 (2012) and Lu et al., Nat. Commun. 2, 578 (2011)].